Energy & Environmental Science

ROYAL SOCIETY OF CHEMISTRY

PAPER

Check for updates

Cite this: *Energy Environ. Sci.*, 2021, **14**, 6041

# Using a vapor-fed anode and saline catholyte to manage ion transport in a proton exchange membrane electrolyzer†

Ruggero Rossi, [a] Derek M. Hall, [b] Le Shi, [a] Nicholas R. Cross, [c] Christopher A. Gorski, [a] Michael A. Hickner [d] and Bruce E. Logan *[ac]

Received 21st July 2021,
Accepted 12th October 2021

DOI: 10.1039/d1ee02265b

rsc.li/ees

Saline water represents an inexhaustible source of water for hydrogen production from electrolysis. However, direct saltwater splitting faces challenges due to chlorine evolution at the anode and the development of Nernst overpotential due to sodium ion transport competition with protons across the membrane. A new approach to minimize chlorine evolution and improve performance is proposed here by using a humidified gas stream (no liquid electrolyte) for the anode and a liquid saltwater catholyte. Charge repulsion of chloride ions by the proton exchange membrane (PEM) resulted in low chlorine generation, with anodic faradaic efficiencies for oxygen evolution of 100 ± 1% with a synthetic brackish water (50 mM NaCl, 3 g $L^{-1}$) and 96 ± 2% with synthetic seawater (0.5 M NaCl, 30 g $L^{-1}$). The enhanced proton transport by the electric field enabled more efficient pH control across the cell, minimizing sodium ion transport in the absence of a liquid anolyte. The vapor-fed anode configuration showed similar performance to a conventional PEM electrolyzer up to 1 A $cm^{-2}$ when both anode and cathode were fed with deionized water. Much lower overpotentials could be achieved using the vapor-fed anode compared to a liquid-anolyte due to the reduced sodium ion transport through the membranes, as shown by adding $NaClO_4$ to the electrolytes. This vapor-fed anode configuration allows for direct use of saltwater in conventional electrolyzers without additional water purification at high faradaic efficiencies.

**Broader context**

Hydrogen gas produced in water electrolyzers requires the use of ultrapure water to avoid contamination of the membrane and the production of hazardous chemicals such as chlorine at the anode. It is shown here that impure, saline water feeds can be used in in a water electrolyzer by feeding the saline liquid into only the cathode chamber and using a vapor feed for the anode, taking advantage of the direction of the electric field and the membrane charge to limit the development of concentration gradients and the generation of chlorine gas. The electrolyzer fed with vapor at the anode and saline water at the cathode showed high faradaic efficiency toward the oxygen evolution reaction, as the $Cl^-$ ions in the catholyte were rejected by the membrane charge, while the electrons transported from anode to cathode limited the diffusion of sodium in the membrane and the development of concentration gradients across the cell. These results show that by using appropriate configuration, impure water feeds can be used in water electrolyzers with little to no change in the cell performance.

## Introduction

Hydrogen gas is a critical component of our energy infrastructure but is typically produced through steam reforming of methane.[1] To reduce fossil fuel consumption and carbon dioxide emissions, hydrogen gas produced by water electrolysis and renewable electricity will become increasingly important as a chemical source for fertilizer production and as an energy carrier for transportation and large-scale grid storage.[2,3] While progress in solar energy technologies has decreased the cost of renewable electricity, providing both a clean and inexpensive source of

[a] *Department of Civil and Environmental Engineering, The Pennsylvania State University, University Park, PA, USA. E-mail: blogan@psu.edu*
[b] *Department of Energy and Mineral Engineering, The Pennsylvania State University, University Park, PA, USA*
[c] *Department of Chemical Engineering, The Pennsylvania State University, University Park, PA, USA*
[d] *Department of Materials Science and Engineering, The Pennsylvania State University, University Park, PA, USA*

† Electronic supplementary information (ESI) available. See DOI: 10.1039/d1ee02265b

electricity, the scarcity of suitable water for electrolysis in many locations remains a challenge.[2,4–7] Typical water electrolyzers use highly purified feeds, requiring ancillary equipment that increases the investments and operational energy costs and overall process complexity. One strategy to avoid these additional expenditures is to develop electrolyzers that are capable of directly using impure water feeds. Around 97% of surface water is saltwater,[8–10] but it has not been directly used for electrolysis due to the production of chlorine gas and reactive species, rather than only oxygen at the anode.[2,7,11] A recent analysis suggested that the overall cost for complete deionization of water is a small percentage of overall costs,[12] but that viewpoint neglected the importance of investment relative to capital costs as well as the impact of intermittent operations due to maintenance of a specialized water treatment operation, which can result in frequent interruptions of hydrogen generation in the electrolysis plant. Thus, it is worthwhile to continue to investigate water electrolysis systems that can use salty water.

In existing PEM water electrolyzers operating under acidic conditions, any appreciable concentration of chloride ions in solution, with most common catalysts, will result high chlorine evolution rates at the anode due to the chlorine evolution reaction (CER) compared to the oxygen evolution reaction (OER).[2,13,14] The CER under acidic pH is typically favored over the OER. While the OER requires a lower thermodynamic potential (1.23 V *vs.* SHE − 0.059 pH) than the CER (1.36 V) at any pH, the kinetic challenges associated with a $4e^-$ transfer OER increases the overpotential for the oxygen evolution well above the potential required to drive chlorine evolution at low pH.[13] The CER is a $2e^-$ transfer reaction, characterized by exchange current density between four to seven orders of magnitude larger than that of the OER.[13] Unfortunately, Ir-based catalysts typically used in PEM electrolyzers, due to their high activity toward the OER, are also extremely active for chlorine evolution, resulting in faradaic efficiencies exceeding 86% for CER in solutions with only 30 mM NaCl.[14] The chlorine generated at the anode, due to its corrosive and volatile nature can drastically reduce the lifetime of the system.[6,10]

A second challenge associated with the use of impaired water for electrolysis is the competition between the cations and protons for the transport of charge across the PEM.[11,15–18] The electrical charge due to the electron flux is typically balanced in PEM electrolyzers by the migration of the protons generated by the OER from the anode to the cathode when pure water is used as a feed. However, when impurities such as sodium ions are present in the electrolytes, electrolyzer performance is drastically reduced.[15,16,19] Cations in the anode chamber such as $Na^+$ compete with protons for transport through the PEM. For each sodium ion migrating across the PEM instead of a proton, an $H^+$ generated by the OER remains in the anode proximity, lowering the local pH.[20] If protons are not effectively supplied to the cathode chamber, the catholyte pH increases due to the generation of hydroxide ions by the HER that are not neutralized by protons based on the following equations:

$$\frac{1}{2}H_2O \leftrightarrow \frac{1}{4}O_2 + H^+ + e^- \quad (1)$$

$$H_2O + e^- \leftrightarrow \frac{1}{2}H_2 + OH^- \quad (2)$$

Thus, large pH differences can develop at the two sides of the PEM, increasing the thermodynamic potential for water splitting. This pH gradient can be described by the Nernst equation, and result in the development of Nernst overpotentials:

$$\begin{aligned} E_{OER} &= E_{0\text{-}OER} - \frac{2.303RT}{F}\log\frac{[O_2]^{\frac{1}{4}}[H^+]}{[H_2O]^{\frac{1}{2}}} \\ &= E_{0\text{-}OER} - \frac{2.303RT}{F}\left[\left(\log\frac{[O_2]^{\frac{1}{4}}}{[H_2O]^{\frac{1}{2}}}\right) - pH\right] \end{aligned} \quad (3)$$

$$\begin{aligned} E_{HER} &= E_{0\text{-}HER} - \frac{2.303RT}{F}\log\frac{[H_2]^{\frac{1}{2}}[OH^-]}{[H_2O]} \\ &= E_{0\text{-}HER} - \frac{2.303RT}{F}\left[\left(\log\frac{[H_2]^{\frac{1}{2}}}{[H_2O]}\right) - 14 + pH\right] \end{aligned} \quad (4)$$

A more acidic pH at the anode will shift the OER potential towards more positive potentials, while a more basic pH at the cathode will decrease the potential of the HER at the cathode. Under equal pH conditions in both chambers the thermodynamic potential difference between OER and HER is 1.23 V (Fig. 1).[15,16] However, if a pH gradient develops, for example an anolyte pH of 3 and a

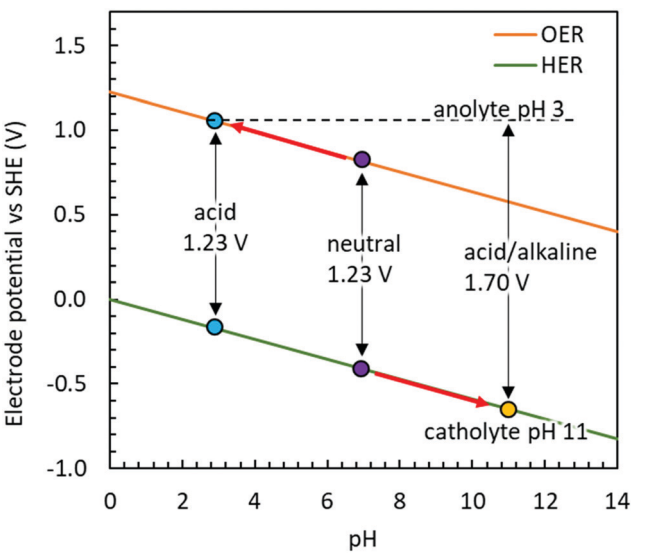


Fig. 1 Impact of anode and cathode pH on the thermodynamic potential for water splitting. The transport of sodium ions instead of protons can led to anode acidification and cathode basification. Each unit of pH difference between anode and cathode increases the overpotential for water splitting by 0.059 V based on the Nernst equation at standard conditions. A decrease in the anode pH from 7 to 3 and an increase in the cathode pH from 7 to 11 raises the thermodynamic potential for water splitting from 1.23 V to 1.70 V.


This journal is © The Royal Society of Chemistry 2021

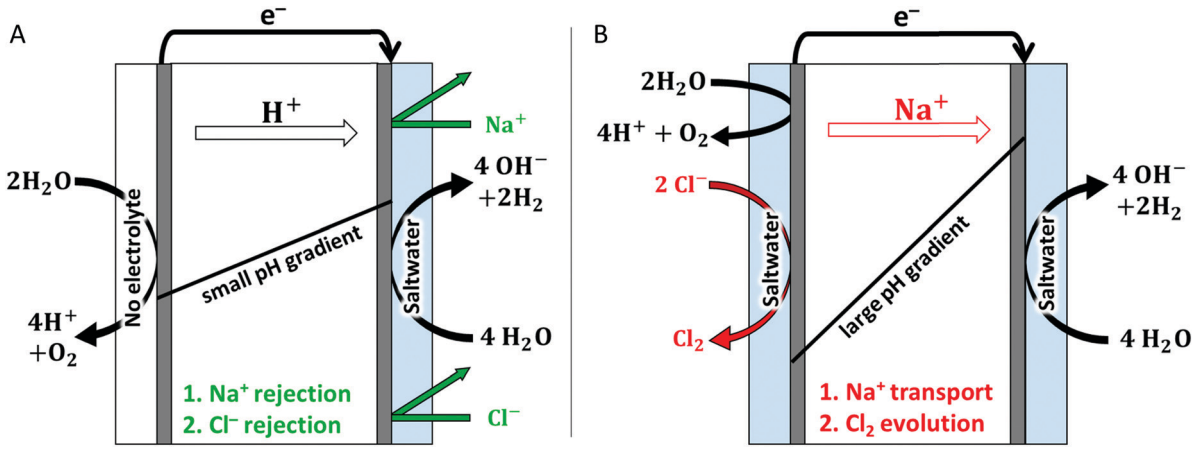


Fig. 2 Comparison between a (A) water electrolyzer using a vapor feed at the anode and saltwater at the cathode and (B) water electrolyzer using saltwater at the anode and the cathode. In the vapor-fed anode configuration, only vapor is fed to the anode chamber and the PEM limits the transport of $Cl^-$ from cathode to anode while the electric field restrict the transport of $Na^+$, avoiding the development of large pH differences across the cell. The combined effect of $Cl^-$ and $Na^+$ repulsion by membrane charge and electric field direction can be obtained only in a PEM electrolyzer (Fig. S1, ESI†).

catholyte pH of 11, then the Nernst overpotential increases the thermodynamic cell voltage to 1.70 V.

In this study, we developed a new and effective water electrolyzer configuration that can accept a saline water as the catholyte feed by using a vapor-fed anode chamber (Fig. 2). The vapor-fed anode leverages the charge of the PEM and the direction of the electric field to limit the intrusion of competing ions into the anode. The negative charges of the sulfonated moieties of the PEM limit the diffusion of $Cl^-$ to the anode by charge repulsion, while the electric field due to the electron transport diminishes the diffusion of sodium ions to the anode as it needs to be balanced by positive ions transported from anode (vapor) to cathode (saltwater), limiting the development of large pH gradients across the PEM.[21] The use of a vapor feeds have previously been investigated in PEM electrolyzers,[22,23] but only by using a configuration different from that examined here. In previous studies water vapor was used as a feed for both the anode and the cathode chambers, but operation under these conditions resulted in an insufficient amount of $H_2O$ reaching the anode, severely limiting the maximum current density of the system to only 0.04 A $cm^{-2}$,[22,23] compared to current densities two orders of magnitude larger for conventional water electrolyzers. In our configuration, the water needed for the OER at the anode is provided by the vapor-feed and by water diffusing from the saline water catholyte through the membrane. The undesirable transport of chloride ions from the catholyte to the anolyte is prevented by charge repulsion of the PEM, while sodium ion transport is minimized by charge transfer of protons from the anode through the PEM, enabling high current densities.

## Materials and methods

### Construction and operation of the water electrolyzer

The cell was a 5 $cm^2$ active area electrolyzer with platinized anode Ti plate and cathode graphite plate with serpentine flow fields (Scribner Associates Inc). The catalyst inks were prepared following a method previously described using a 20% ionomer/catalyst ratio for the cathode and a 25% ionomer/catalyst ratio for the anode.[24] Iridium black (Alfa Aesar) was used as received as catalyst for the OER on the anode and painted on a Ti felt (thickness: 250 ± 50 μm, Fuel Cell Store) with loadings of 5 mg $cm^{-2}$. Pt on Vulcan XC72 carbon (20 wt% Pt/C, BASF) was sprayed with loadings of 2.5 mg $cm^{-2}$ on carbon cloth (1071 HCB, 356 μm, Fuel Cell Store) for the HER. The membrane electrode assembly (MEA) was fabricated by hot-pressing the electrode onto Nafion® 117/212 membranes for 2 min at 130 °C at a pressure of 3000 psi. The cell was sealed at 11.5 N m with two 254 μm thick PTFE gaskets (Scribner Associates Inc). Cell and reactant inlet temperatures were set at 80 °C.

Deionized (DI) water or a solution of sodium perchlorate 10 mM was used as the electrolyte for the liquid-anolyte electrolyzer to avoid chlorine evolution in some experiments. DI water, sodium perchlorate 10 mM, or sodium chloride (50 mM or 0.5 M) were used as catholytes in the vapor-fed anode electrolyzer and pumped at 25 mL $min^{-1}$ except otherwise noted. The gas feed to the anode in the vapor-fed anode configuration was saturated with water vapor by bubbling it at a flow rate of 25 mL $min^{-1}$ through a reservoir that had been filled with DI and maintained at 80 °C. The humidified gas stream was directly pumped in the anode chamber of the vapor-fed anode electrolyzer. Ambient pressure was used for all tests. The pH (Mettler Toledo) and the chlorine content (LaMotte Benchtop chlorine meter – diethyl-*p*-phenylene diamine (DPD) colorimetric test) of the electrolytes were measured after tests and analyzed immediately. The faradaic efficiency (FE) was calculated by (1) water displacement and (2) analysis with gas chromatography (GC, SRI Instrument, Torrance, CA, USA) injecting 250 μL of gas collected with gas bags with an airtight syringe (Hamilton, Reno, NV, USA).

### Electrochemical characterization

The electrochemical tests were performed with a Gamry 3000 potentiostat. The polarization curves were recorded with linear sweep voltammetries (LSVs) at a scan rate of 10 mV $s^{-1}$ until at

least three reproducible cycles were obtained. AC impedance measurements were recorded after the LSVs in a range of 50 kHz–10 mHz at different applied potentials. A chronoamperometry (CA) was performed following the impedance measurements at 0.5 A $cm^{-2}$ to investigate the impact of a constant current on the cell performance. In these measurements, only current densities of up to 0.6 A $cm^{-2}$ were achieved due to limitations in the potentiostat used. In a different set of experiments, a power supply (GWInstek GPR-1820 HD) was used to obtain CAs at 1 A $cm^{-2}$ in the liquid-anolyte and vapor-anode configurations. Sodium perchlorate 10 mM, sodium chloride 50 mM and 0.5 M was added in the catholyte at different time during the CA. The cell voltage was recorded with a MPG2 Bio-logic potentiostat.

## Results and discussion

### Vapor-fed anode *versus* liquid-anolyte electrolyzer performance

The vapor-fed anode configuration produced similar overpotentials relative to those measured using deionized water as liquid anolyte, while it substantially improved performance in the presence of sodium ions based on measured overpotentials. Using DI water at a set current of 1 A $cm^{-2}$, the cell voltage of the vapor-fed anode configuration averaged 1.74 ± 0.01 V (Fig. 3A), similar to that of a cell with liquid electrolytes feed in the anode and cathode chambers of 1.77 ± 0.01 V (Fig. 3B). The extra energy needed for heating the water reservoir used to produce the water vapor fed to the anode is negligible compared to the energy consumed to operate the electrolyzer. Considering a vapor feed of 25 mL $min^{-1}$, or 0.92 g $h^{-1}$, the energy needed to heat the water will be 0.064 W h, which corresponds to only 0.7% of the 8.7 W h needed to sustain a voltage of 1.74 V at a current of 5 A (1 A $cm^{-2}$) for one hour. To examine the impact of sodium ions on the cell overpotential, in the absence of current production from chloride ion oxidation, 10 mM $NaClO_4$ was added to the liquid electrolytes. The presence of sodium ions increased the cell voltage of the vapor anode electrolyzer by 9% (by 0.16 V to 1.90 ± 0.01 V), compared to a much larger increase of 40% (0.67 V) for the liquid-anolyte electrolyzer (2.44 ± 0.00 V). The use of a vapor-fed anode has been proposed in previous

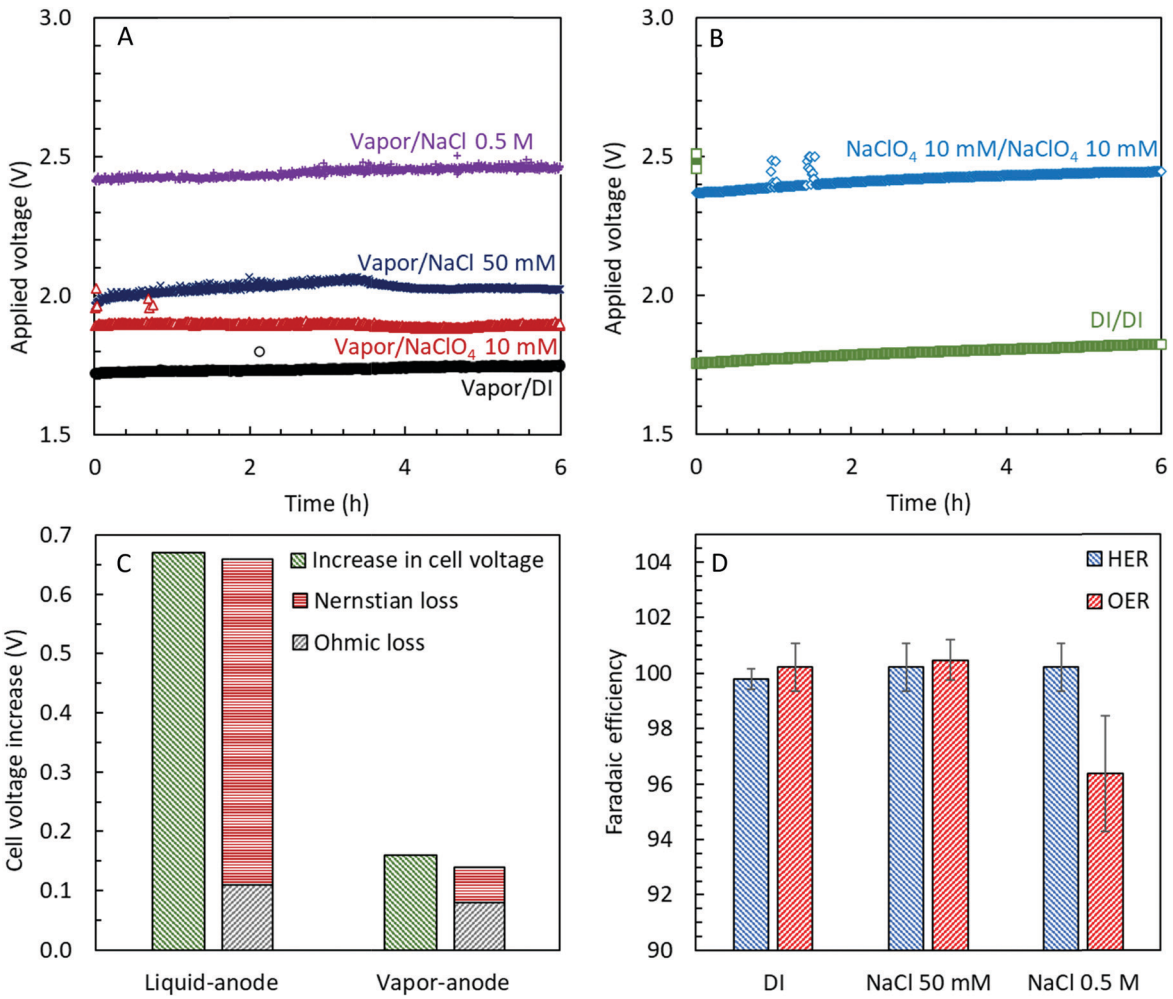


Fig. 3 Chronoamperometries at 1 A $cm^{-2}$ of the (A) vapor-fed anode and (B) liquid-fed anode electrolyzer using Nafion 212 with different concentrations of $NaClO_4$ and NaCl in the electrolyte. (C) Impact of the presence of sodium ions in solution in terms of overpotential due to pH gradient, calculated from the Nernst equation, and ohmic losses, calculated from the Ohm's law. (D) Faradaic efficiency of the vapor-fed anode electrolyzer with different NaCl concentration in the catholyte.

 This journal is © The Royal Society of Chemistry 2021

studies,[22,23] however, it was coupled with a vapor-fed or a dry ($N_2$ gas) fed cathode, which failed to provide sufficient water for the OER and the HER. As a result, the limiting current densities were around two orders of magnitude ($\sim$0.04 A cm$^{-2}$) lower than that those obtained here by coupling the vapor-fed anode with a saltwater feed catholyte.

The largest impact of the sodium ion on performance was the increased Nernst overpotential due to pH gradient across the cell. With current generation, the electric field enhanced the migration of positive ions from anode to cathode through the PEM to balance charge. However, the concentration of sodium ions in solution (10 mM using $NaClO_4$) is larger than that of protons (0.001 mM at pH 6), and their transport across the membrane is therefore favored. When a sodium ion, rather than a proton, migrates from anode to cathode to balance charge, the anolyte pH decreases (eqn (1)) and the catholyte pH increases due to the release of hydroxide ions (eqn (2)) that are not neutralized by protons.[15,16,25] Thus, a large pH gradient develops across the PEM, resulting in Nernst overpotentials due to the pH differences in the cell (Fig. 1). In the liquid-anolyte configuration, using $NaClO_4$ (10 mM) to study the impact of $Na^+$ ions separately from impacts of the CER, the solution pH shifted from a pH of 6.0 in both electrolytes to 2.5 in the anolyte and to 11.9 in the catholyte. This produced a pH difference of 9.4 units of pH across the PEM and increased the overpotential calculated from the Nernst equation by 0.55 V, representing the largest portion of the voltage increase due to $NaClO_4$ addition (0.67 V) (Fig. 3C). Using the vapor-fed anode configuration produced a smaller pH gradient across the PEM as shown by a cathode increase in pH from 5.9 to 6.9, corresponding to an increase in the Nernstian overpotential of only 0.06 V (Fig. 3C). The relatively small overpotential of the vapor-fed anode configuration with $NaClO_4$ (0.16 V), indicated that the electric field limited the intrusion of sodium ions in the anode chamber, and therefore the development of concentration gradients and Nernst overpotential which was detrimental for the efficient operation of the cell.

A small portion of the increase in overpotential due to sodium in solution was related to an increase in the PEM resistance.[26–28] Sodium ions have higher affinity than protons toward the sulfonic groups of the PEM, thus lower membrane diffusivity, increasing the resistance of the membrane in ion transport.[27,28] The EIS analysis with sodium perchlorate in solution revealed that the ohmic resistance of the liquid-anolyte electrolyzer was 61% higher (0.29 Ω cm$^2$) than that obtained using deionized water (0.18 Ω cm$^2$) (Fig. 3C and Fig. S3, ESI†). This higher resistance with sodium in the electrolyte therefore contributed up to 0.11 V to the cell overpotential at 1 A cm$^{-2}$, or about 18% of the increased in overpotential by using $NaClO_4$ in the liquid-anolyte electrolyzer (Fig. 3C). Using the vapor-fed anode configuration promoted proton migration from the anode through the PEM, achieving minimal sodium ion diffusion into the membrane, as shown by a smaller increase of the ohmic resistance in the vapor-fed anode configuration (44%, from 0.18 Ω cm$^2$ to 0.26 Ω cm$^2$) compared to the liquid-anolyte configuration, corresponding to an overpotential of 0.08 V, contributing to 50% of the increased overpotential (Fig. 3C). In the vapor-fed anode configuration, due to the absence of the electrolyte in the anode chamber, the sodium ions are continuously replenished only in the cathode chamber, and their diffusion in the membrane is minimized by the electric field, which favors the migration of positive ions from anode to cathode. Thus, the protons generated by the OER at the anode are primarily used for maintaining charge balance across the cell, and the water required by the OER is provided by the vapor stream and transport across the PEM.

The much larger impact of the increased Nernst overpotential than that due to a reduction in membrane conductivity is analogous to that previously reported for pH shifts in anion exchange membrane fuel cells (AEMFC) due to bicarbonate ion transport.[29] In that study it was found that the bicarbonate from $CO_2$ can compete with the hydroxide ions for transport across the AEM, increasing the cell overpotential. Adding 400 ppm of $CO_2$ at 1 A cm$^{-2}$ increased the overpotential by 281 mV, with only 9% (25 mV) due to the decrease in membrane conductivity. The largest portion (58%, 162 mV) of the increased overpotential resulted from the Nernst overpotential due to concentration gradient, with the remainder caused by charge transfer losses (33%, 94 mV). The same relative decreases in overpotentials resulted here using two liquid electrolytes with $Na^+$ ions in solution where the greatest proportion of the increased electrolyzer overpotential was due to the development of a pH gradient compared to a much smaller overpotential due to the increased membrane resistance.

### Using a saltwater catholyte in the vapor-fed anode electrolyzer

We investigated the faradaic efficiency toward the OER using sodium chloride solutions representative of brackish water (NaCl 50 mM, 3 g L$^{-1}$) and seawater (NaCl 0.5 M, 30 g L$^{-1}$). When chloride ions were used in the liquid catholytes there was no significant amount of chlorine generation in the vapor-fed anode electrolyzer based on the measured faradaic efficiencies. The vapor-fed anode electrolyzer had a faradaic efficiency of 100 ± 1% for oxygen using impaired water (50 mM NaCl) in the feed at current densities up to 1 A cm$^{-2}$ (Fig. 3D). Even though the FE with NaCl 50 mM averaged 100% for the anode, small traces of $Cl_2$ were generated as shown by a small amount of $Cl_2$ detected in the anode liquid reservoir (4.5 ± 0.4 μmol h$^{-1}$), equivalent to 0.1% of the FE. Therefore, under these conditions there was very little transport of chloride ions from the catholyte to the anode. Tests were not conducted using NaCl solutions in both chambers in order to avoid damage to the system that would result from very high chlorine generation rates.

Even at NaCl concentrations analogous to salt concentrations in seawater (0.5 M NaCl), faradaic efficiencies remained very high (96 ± 2%) in the vapor-fed anode electrolyzer. The much higher chloride concentrations in the cathode chamber with 0.5 M NaCl resulted in more substantial $Cl^-$ transport across the PEM into the anode chamber that resulted in the reduced FE. Based on the decrease in the FE the amount of $Cl_2$ produced with NaCl 0.5 M was 1.9 mmol h$^{-1}$, but only a small fraction (24.8 ± 0.5 μmol h$^{-1}$ corresponding to 0.5% FE) of it was detected in the

anolyte reservoir likely due to volatilization or oxidation of the electrolyzer components.

Sodium ions in the NaCl 50 mM solution increased the cell overpotential due to the development of a pH gradient across the cell. In the vapor-fed anode electrolyzer fed NaCl 50 mM the cell voltage was 0.29 V (2.03 ± 0.01 V) larger than that obtained with a DI catholyte (1.74 ± 0.01 V), although this was 0.41 V lower than the cell voltage of the liquid-anolyte electrolyzer with a lower sodium concentration of 10 mM $NaClO_4$ (2.44 ± 0.00 V) (Fig. 3A and B). Larger concentrations of NaCl (0.5 M) substantially increased the cell voltage to 2.45 ± 0.02 V. Each increase in the cell overpotential was accompanied by an increase in the pH gradient across the PEM. The pH difference between anode and cathode was 3.4 units of pH with NaCl 50 mM, corresponding to a Nernst overpotential due to that pH gradient of 0.20 V. With 0.5 M NaCl, the pH difference between anode and cathode increased to 8 units of pH (anode pH of 2.9 and a cathode pH of 11.3), increasing the Nernst overpotential by 0.5 V. Thus, the development of a pH gradient in the vapor-fed anode configuration was affected by the sodium concentration in the cathode chamber.

### Impact of sodium ions on the vapor-fed anode electrolyzer performance with Nafion 117

The impact of the presence of sodium ions in solution on electrolyzer overpotentials was investigated with a thicker membrane (Nafion 117, 183 μm) using different $NaClO_4$ concentrations in the catholyte. The cell voltage in the vapor-fed anode configuration was not affected by $NaClO_4$ concentrations up to 10 mM (1.62 V) but it increased by 0.11 V with 0.1 M $NaClO_4$ (1.73 V) compared to DI (1.62 V) (Fig. 4A and B). The voltage of the vapor-fed electrolyzer using 1 M $NaClO_4$ as a catholyte initially increased up to 2.19 V and then slowly diminished until reaching 1.87 V (0.25 V additional voltage compared to DI), likely due to the purging of the sodium ions which entered the membrane during startup. These cell voltages are all lower than those obtained when feeding the same solutions containing $NaClO_4$ into the liquid anolyte. The cell voltage was 0.55 V larger (2.16 V) using a 10 mM $NaClO_4$ solution as the anolyte and catholyte compared to the same configuration with DI (1.62 V). The overpotentials due to sodium transport in the vapor-fed anode electrolyzer with Nafion 117 were also lower than those obtained with the thinner Nafion 212 in $NaClO_4$ solutions (Fig. 3A and B). With the thinner Nafion 212 (50.8 μm), the cell voltage increased by 0.16 V with 10 mM $NaClO_4$ in the catholyte, compared to no change in the cell voltage using the same solution with Nafion 117. The electrolyzer voltage increased by only 0.11 V in a 10× more concentrated $NaClO_4$ solution (0.1 M). Thus, using thicker PEMs (Nafion 117 instead of Nafion 212) limited the development of large overpotentials in the presence of high concentration of sodium ions in the vapor-fed anode configuration. Therefore, the concentration gradient that developed across the cell depends on the thickness of the PEM separating the electrodes.

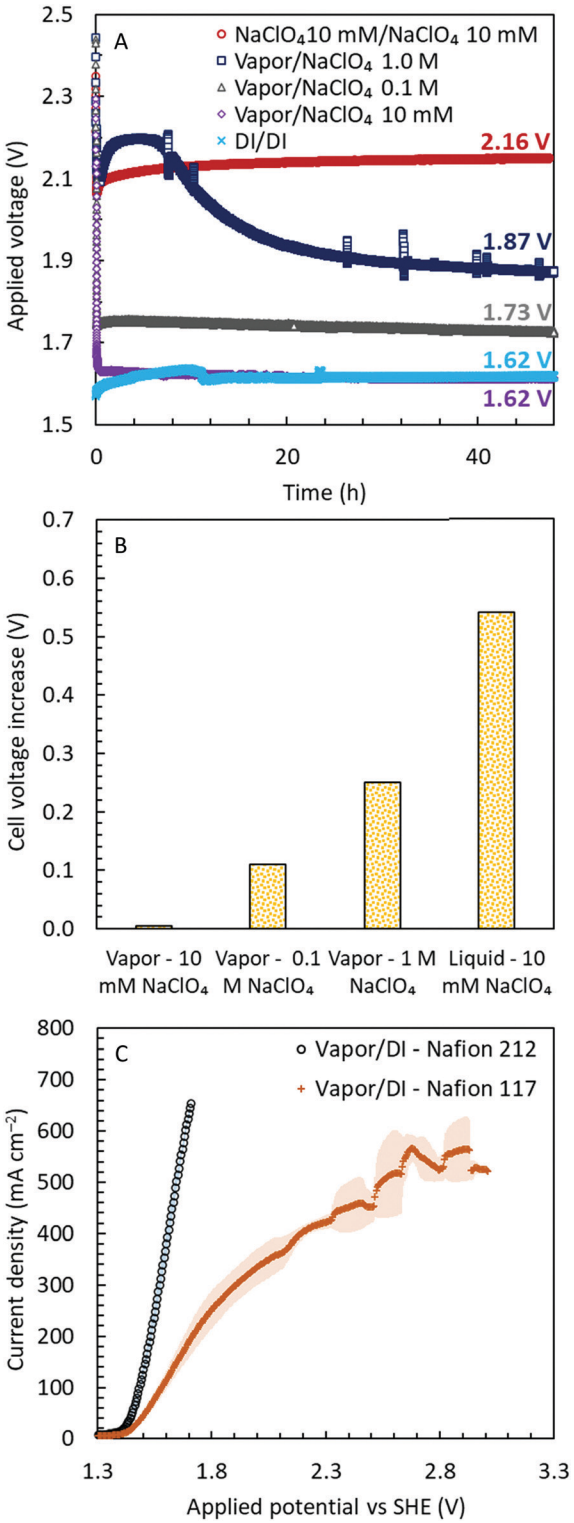


Fig. 4 (A) Chronoamperometries at 60 mA $cm^{-2}$ and (B) correspondent overpotentials due to sodium with different concentration of $NaClO_4$ in the catholyte of the vapor-fed anode electrolyzer compared to a liquid-anolyte electrolyzer fed with DI in anode and cathode chambers separated by Nafion 117. (C) Linear sweep voltammetries in the vapor-fed anode configuration with different membrane thicknesses. Increasing the PEM membrane thickness from 51 μm (Nafion 212) to 183 μm (Nafion 117) result in the development of a mass-transfer controlled regime at high current densities.


This journal is © The Royal Society of Chemistry 2021

Using Nafion 117 limited the maximum current density that can be delivered by the vapor-fed electrolyzer, despite the reduced cell overpotentials in the presence of sodium ions. While no apparent limiting current density was reached with Nafion 212 (50.8 μm) up to 1 A $cm^{-2}$, a maximum current density of 0.6 A $cm^{-2}$ was obtained using Nafion 117 (183 μm), likely due to the reduced water flux from the cathode to anode (Fig. 4C). This limiting current density is slightly lower than that previously obtained (0.8 A $cm^{-2}$) when pure water was fed only at the cathode of an electrolyzer using Nafion 117. In that study, when Nafion 117 was replaced with Nafion 212, the limiting current density increased to 2.4 A $cm^{-2}$.[30] The transport of water through the PEM depends on the pressure in the cathode chamber and the thickness of the membrane.[30,31] The OER consumes water (eqn (1)), thus maintaining sufficient water at the anode through humidification and diffusion through the membrane is critical for operation of the electrolyzer (Fig. S4, ESI†).[30] In the vapor-fed anode electrolyzer, water molecules can diffuse from the cathode to the anode due to the concentration gradient, and the humidified gas stream contributes in keeping the anode wet and provide $H_2O$ molecules for the OER.[22] However, each proton migrating under the effect of the electric field transports 1–3 water molecules away from anode to the cathode.[32,33] At high currents, the migration of ions coupled with water consumption by the OER will increase water losses relative to that provided by the humidified air or water diffusion from the cathode, drying the anode and PEM, limiting the electrolyzer performance. Thus, a trade-off exists in the choice of the PEMs in the vapor-fed anode configuration, with thinner membranes enabling higher current densities of the electrolyzer but allowing higher sodium ion transport to the anode compared to thicker membranes. The sodium ions in the anode chamber

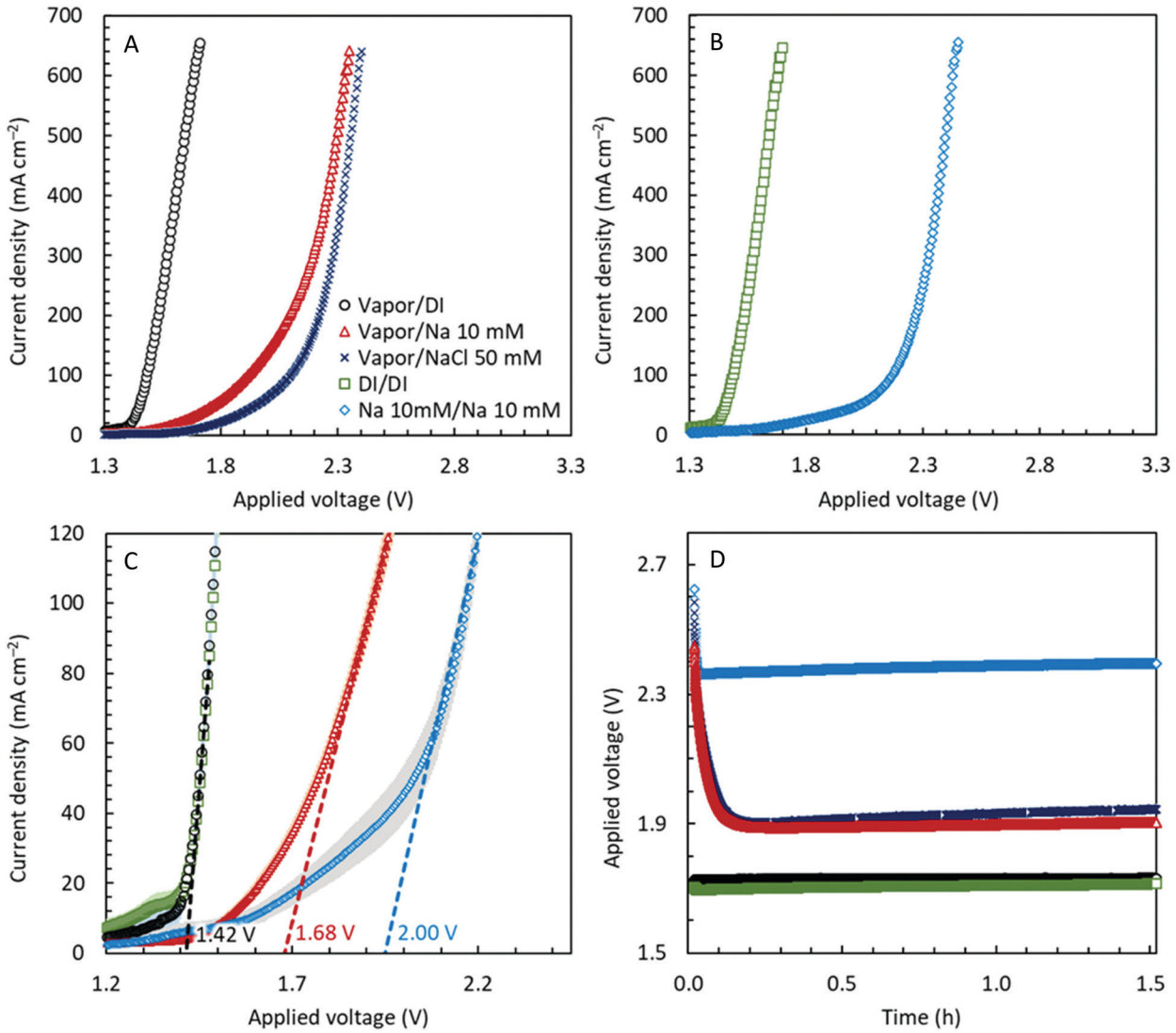


Fig. 5 LSVs of the (A) vapor-fed anode and (B) liquid-anolyte configurations containing different sodium concentrations in solution. (C) Onset potentials for the vapor-fed anode and liquid-anolyte configurations fed electrolytes with different ionic concentrations based on the linear region as shown. The current density range used for the linearization was 80–120 mA $cm^{-2}$. (D) Chronoamperometries at 0.5 A $cm^{-2}$ with different concentration of ions in the electrolyte fed to both anode and cathode or only at the cathode.

can migrate back in the cathode chamber under the effect of the electric field, contributing to increase the cell overpotentials due to the development of pH gradients across the cell.

#### Electrochemical characterization of the vapor-fed anode electrolyzer

The vapor-fed anode electrolyzer showed similar performance in LSVs compared to the liquid-anolyte electrolyzer when fed with ultrapure water (Fig. 5A and B). The cell voltage of the liquid-anolyte electrolyzer fed DI water was 1.64 V at 0.5 A $cm^{-2}$, similar to that obtained in the vapor-fed anode configuration (1.65 V at 0.5 A $cm^{-2}$). Adding as low as 10 mM sodium perchlorate in the solution of a liquid-anolyte electrolyzer increased the cell voltage at 0.5 A $cm^{-2}$ of 0.8 V to 2.40 V compared to a DI/DI configuration (1.64 V) (Fig. 5B). The vapor-fed anode electrolyzer produced similar current densities of the liquid-anolyte electrolyzer at voltages around 0.1 V smaller. For example, at 0.5 A $cm^{-2}$ the cell voltage of the vapor-fed anode electrolyzer was 2.30 V, but further increasing the concentration of sodium to 50 mM and 0.5 M increased the cell voltage to 2.37 V, similar to that obtained in the liquid-anolyte configuration with sodium 10 mM (2.40 V) (Fig. 5A). Using sodium perchlorate 10 mM as electrolyte shifts the onset voltage by more than 0.6 V from 1.42 V to 2.00 V for the liquid-anolyte configuration and by 0.3 V for the vapor-fed anode electrolyzer compared to the configurations using pure water (Fig. 5C).

The shift in the onset voltage of 0.3 V for the vapor-fed anode configuration with 10 mM sodium perchlorate as a catholyte was larger than the cell voltage shift obtained in the chronoamperometry at 1 A $cm^{-2}$ (Fig. 3A and B). Thus, we investigated the impact on the cell voltage of the application of a constant current in the different electrolyzer configurations. Driving constant current through the vapor-fed anode electrolyzer reduced the cell overpotential when sodium ions were present in the catholyte over time (Fig. 5D). At 0.5 A $cm^{-2}$ the cell voltage decreased from 2.45 V to 1.90 V with sodium perchlorate 10 mM and from 2.55 V to 1.93 V with NaCl 50 mM after only one hour of operation. Such cell voltages were 0.2 V larger with $NaClO_4$ 10 mM and NaCl 50 mM compared to that obtained with ultrapure water and similar to that obtained in the chronoamperometry at 1 A $cm^{-2}$ (0.2 V with $NaClO_4$ 10 mM and 0.2 V with NaCl 50 mM), indicating that constant currents shall be applied to completely exploit the advantages of the vapor-fed anode configuration in decreasing the cell overpotentials. The decrease in the cell voltage over time was likely due to the progressive removal of sodium ions from the PEM under the effect of the electric field, contributing to diminish the development of large differences of pH between anode and cathode. The voltages of the liquid-anolyte configuration fed ultrapure water or sodium perchlorate 10 mM did not change during the chronoamperometry (Fig. 5D).

## Conclusions

Using a vapor-fed anode configuration and a saltwater catholyte minimized chlorine generation in the anode chamber, leveraging the selectivity of the PEM in rejecting the chloride ions from the cathode chamber. A faradaic efficiency of 100 ± 1% was obtained using NaCl 50 mM (3 g $L^{-1}$) as a catholyte, and it was reduced to only 96 ± 2% with NaCl 0.5 M (30 g $L^{-1}$). The use of specific anode catalysts that minimize the CER could further reduce the generation of chlorine in these vapor-fed anode electrolyzers. The absence of a liquid anolyte limited the sodium diffusion through the PEM, as positive ions were primarily migrating from anode to cathode to balance the charge, avoiding the development of large pH gradients across the PEM. The cell voltage increased by only 9% (vapor-DI, 1.74 ± 0.01 V; vapor-$NaClO_4$ 10 mM, 1.90 ± 0.01 V) in a vapor-fed anode configuration, compared to a much larger increase of 40% for the electrolyzer fed with a liquid anolyte containing sodium ions (DI–DI, 1.77 ± 0.01 V; $NaClO_4$ 10 mM–$NaClO_4$ 10 mM, 2.44 ± 0.00 V), due to a lower pH gradient in the vapor-fed anode configuration (1 unit of pH) compared to the liquid-anolyte configuration (9 units of pH). Using thicker PEMs (Nafion 117–183 μm *vs.* Nafion 212–50.8 μm) in the electrolyzer allowed to further diminish the overpotential due to sodium contamination but lowered the maximum current density to 0.6 A $cm^{-2}$ in the vapor-fed anode configuration. This new configuration can advance current PEM electrolyzer technologies towards the use of impaired waters as it showed that commercial water electrolyzer with PEM can be used with a seawater feed with little to no modification in the system architecture at current densities relevant for their application. The stability over several months and the complete suppression of the CER with dedicated anode catalysts will be next technical challenge for development of a practical system.

## Conflicts of interest

The authors declare no competing interests.

## Acknowledgements

The authors acknowledge funding by Penn State University and the National Science Foundation CBET-2027552.

## References

1 F. B. Bendixen, W. L. Eriksen, K. Aasberg-petersen, C. Frandsen, I. Chorkendorff and P. M. Mortensen, *Science*, 2019, **759**, 756–759.
2 W. Tong, M. Forster, F. Dionigi, S. Dresp, R. Sadeghi Erami, P. Strasser, A. J. Cowan and P. Farràs, *Nat. Energy*, 2020, **5**, 367–377.
3 J. N. Galloway, A. R. Townsend, J. W. Erisman, M. Bekunda, Z. Cai, J. R. Freney, L. A. Martinelli, S. P. Seitzinger and M. A. Sutton, *Science*, 2008, **320**, 889–892.
4 Y. Kuang, M. J. Kenney, Y. Meng, W. H. Hung, Y. Liu, J. E. Huang, R. Prasanna, P. Li, Y. Li, L. Wang, M. C. Lin, M. D. McGehee, X. Sun and H. Dai, *Proc. Natl. Acad. Sci. U. S. A.*, 2019, **116**, 6624–6629.

 This journal is © The Royal Society of Chemistry 2021

5 L. Yu, Q. Zhu, S. Song, B. McElhenny, D. Wang, C. Wu, Z. Qin, J. Bao, Y. Yu, S. Chen and Z. Ren, *Nat. Commun.*, 2019, **10**, 1–10.

6 L. Shi, R. Rossi, M. Son, D. M. Hall, M. A. Hickner, C. A. Gorski and B. E. Logan, *Energy Environ. Sci.*, 2020, **13**, 3138–3148.

7 S. Dresp, F. Dionigi, M. Klingenhof and P. Strasser, *ACS Energy Lett.*, 2019, **4**, 933–942.

8 S. Khatun, H. Hirani and P. Roy, *J. Mater. Chem. A*, 2021, **9**, 74–86.

9 F. Dionigi, T. Reier, Z. Pawolek, M. Gliech and P. Strasser, *ChemSusChem*, 2016, **9**, 962–972.

10 S. S. Veroneau and D. G. Nocera, *Proc. Natl. Acad. Sci. U. S. A.*, 2021, **118**, 1–5.

11 S. Dresp, T. Ngo Thanh, M. Klingenhof, S. Brückner, P. Hauke and P. Strasser, *Energy Environ. Sci.*, 2020, **13**, 1725–1729.

12 J. N. Hausmann, R. Schlögl, P. W. Menezes and M. Driess, *Energy Environ. Sci.*, 2021, **14**, 3679–3685.

13 J. G. Vos and M. T. M. Koper, *J. Electroanal. Chem.*, 2018, **819**, 260–268.

14 J. G. Vos, T. A. Wezendonk, A. W. Jeremiasse and M. T. M. Koper, *J. Am. Chem. Soc.*, 2018, **140**, 10270–10281.

15 L. Zhang, X. Jie, Z. G. Shao, Z. M. Zhou, G. Xiao and B. Yi, *Int. J. Hydrogen Energy*, 2012, **37**, 1321–1325.

16 L. Zhang, X. Jie, Z. G. Shao, X. Wang and B. Yi, *J. Power Sources*, 2013, **241**, 341–348.

17 S. Dresp, F. Dionigi, S. Loos, J. Ferreira de Araujo, C. Spöri, M. Gliech, H. Dau and P. Strasser, *Adv. Energy Mater.*, 2018, **8**, 1800338.

18 C. Xiang, K. M. Papadantonakis and N. S. Lewis, *Mater. Horiz.*, 2016, **3**, 169–173.

19 B. L. Kienitz, H. Baskaran and T. A. Zawodzinski, *Electrochim. Acta*, 2009, **54**, 1671–1679.

20 R. A. Rozendal, T. H. J. A. Sleutels, H. V. M. Hamelers and C. J. N. Buisman, *Water Sci. Technol.*, 2008, **57**, 1757–1762.

21 G. M. Geise, H. J. Cassady, D. R. Paul, B. E. Logan and M. A. Hickner, *Phys. Chem. Chem. Phys.*, 2014, **16**, 21673–21681.

22 J. M. Spurgeon and N. S. Lewis, *Energy Environ. Sci.*, 2011, **4**, 2993–2998.

23 S. Kumari, R. Turner White, B. Kumar and J. M. Spurgeon, *Energy Environ. Sci.*, 2016, **9**, 1725–1733.

24 W. Xu and K. Scott, *Int. J. Hydrogen Energy*, 2010, **35**, 12029–12037.

25 R. A. Rozendal, H. V. M. Hamelers and C. J. N. Buisman, *Environ. Sci. Technol.*, 2006, **40**, 5206–5211.

26 I. A. Stenina, P. Sistat, A. I. Rebrov, G. Pourcelly and A. B. Yaroslavtsev, *Desalination*, 2004, **170**, 49–57.

27 J. G. Goodwin, K. Hongsirikarn, S. Greenway and S. Creager, *J. Power Sources*, 2010, **195**, 7213–7220.

28 T. Okada, H. Satou, M. Okuno and M. Yuasa, *J. Phys. Chem. B*, 2002, **106**, 1267–1273.

29 Y. Zheng, T. J. Omasta, X. Peng, L. Wang, J. R. Varcoe, B. S. Pivovar and W. E. Mustain, *Energy Environ. Sci.*, 2019, **12**, 2806–2819.

30 M. Müller, M. Carmo, A. Glüsen, M. Hehemann, S. Saba, W. Zwaygardt and D. Stolten, *Int. J. Hydrogen Energy*, 2019, **44**, 10147–10155.

31 Q. Duan, H. Wang and J. Benziger, *J. Membr. Sci.*, 2012, **392–393**, 88–94.

32 Y. K. Choe, E. Tsuchida, T. Ikeshoji, S. Yamakawa and S. A. Hyodo, *J. Phys. Chem. B*, 2008, **112**, 11586–11594.

33 T. A. Zawodzinski, C. Derouin, S. Radzinski, R. J. Sherman, V. T. Smith, T. E. Springer and S. Gottesfeld, *J. Electrochem. Soc.*, 1993, **140**, 1041–1047.